Science Arts & Métiers (SAM)

is an open access repository that collects the work of Arts et Métiers Institute of Technology researchers and makes it freely available over the web where possible.

To cite this version :

Development of a numerical model for the understanding of the chip formation in high-pressure water-jet assisted machining

Y. Ayed [a,*], C. Robert [a], G. Germain [a], A. Ammar [a,b]

[a] Arts et Métiers ParisTech, LAMPA, 2 bd du Ronceray, 49035 Angers Cedex, France
[b] UMSSDT, ENSIT, Université de Tunis, 5 Avenue Taha Hussien, Monteury 1008, Tunis, Tunisie

ABSTRACT

The aim of this study is to develop a new numerical cutting model that includes fluid structure interaction and to take into account heat transfer between the water-jet, the workpiece and the chip. This has been achieved using a CEL (Coupled–Eulerian–Lagrangian) technique, an algorithm has been developed to ensure heat exchange between the fluid and the structure. This new model allows decoupling of the mechanical and the thermal effects of the water-jet on chip formation and fragmentation. It has been demonstrated that fragmentation of the chip is ensured by the combination of the thermal and the mechanical effects of the water-jet. Moreover, the tool rake temperature is reduced by more than 400 °C, the tool/chip contact length is also decreased by about 30%.

1. Introduction

Understanding the thermo-mechanical mechanisms involved in chip formation, during machining operations, is very challenging. Indeed, the very localized cutting area makes it difficult to access and to experimentally observe the cutting process. Moreover, this zone is subjected to very high mechanical and thermal gradients. For high-pressure water-jet assistance, observations are not possible because of the interference created by spray from the water-jet.

Numerical modeling is therefore an important research tool, in order to contribute to the understanding of this phenomenon. However, the model must represent, as accurately as possible, the physical phenomena involved in metal cutting such as friction, material behavior and the interaction between the water-jet, the workpiece and the tool. This model, once validated, allows the understanding of the mechanical and the thermal actions of the water-jet on chip formation. It also enables the prediction of cutting forces, temperature fields, chip morphology and chip fragmentation.

The numerical modeling of assisted machining operations is often very difficult due to the strong multi-physics coupling involved. The modeling of laser assistance occupies a dominant part of the research in the field of numerical simulation of machining assistance [18,29,5,10,11,9,33]. There is also almost a total lack of work concerning the modeling cryogenic and high-pressure water-jet assistance. Only a few studies have been focused on this type of simulation, but none have taken into account the fluid structure interaction, making them very simplistic [8]. In order to simulate the high speed water-jet, the Hugoniot equation of state is often employed. The water-jet is regarded as an incompressible fluid. The Coupled Eulerian Lagrangian (CEL) method has been used by [12,24,23,15,17] to simulate the fluid/structure interaction and material erosion under water-jet impact. It has been also used to simulate tube forming and water-jet spot welding [6,7].

To improve the existing cutting models, researchers implement new material constitutive models giving better predictions of the cutting forces and the physical phenomena. The research conducted by [19,20,25] is based on a physical model that allows the simulation of the dislocation density and the grain refinement during the machining operation. In addition, this model permits the prediction of the machined surface hardness. A constitutive model based on the self-consistent method (SCM) has been used by [32] in order to capture the state of the material and its phase transformation. Reference [4] used a modified Bai–Wierzbicki material model for a more accurate prediction of chip formation. New studies are also focused on the numerical simulation of tool wear [28,16,30]. This type of study presents particular challenges due to the complexity of the wear mechanisms.

* Corresponding author.
  E-mail address: yessine.ayed@ensam.eu (Y. Ayed).

2. Numerical model

The aim of this section is to present the numerical cutting model that takes into account the fluid/structure interaction and the heat transfer between the water-jet, the workpiece and the tool.

Modeling of the fluid/structure interaction with ABAQUS has been carried out with the Coupled-Eulerian–Lagrangian (CEL) method. This method consists of using an Eulerian formulation for the fluid and a Lagrangian formulation for the structure.

In order to simulate the machining process, it is necessary to rely on a constitutive law and a damage model that can take into account the high temperatures and dynamic behavior of the material. Therefore the constitutive law of Johnson–Cook [13] and the Johnson–Cook damage model [14] have been chosen. Indeed, the mathematical simplicity and the ease of identification, combined with good prediction accuracy of the physical phenomena, is a significant advantage.

This constitutive law is shown in Eq. (1). The first term represents the isotropic hardening of Ludwik [21]. The second term represents the sensitivity to the strain rate. The temperature sensitivity is represented by the third term. The parameters A, B, n, C, m are constants that must be determined experimentally, via tests over a wide range of temperatures and strain rates. $\dot{\varepsilon}_0$, T_m and T_a represent the reference strain rate, the melting temperature of the material and the ambient temperature, respectively

$$\sigma = \underbrace{(A+B^n)}_{1}\underbrace{\left(1+C\ln\frac{\dot{\varepsilon}}{\dot{\varepsilon}_0}\right)}_{2}\underbrace{\left(1-\left(\frac{T-T_a}{T_f-T_a}\right)^m\right)}_{3} \tag{1}$$

The damage model relates the fracture strain to the triaxiality, the strain rate and the temperature. Thus, the fracture strain is written in the form of Eq. (2). The first, the second and the third term represent the sensibility of the fracture strain to the triaxiality, the strain rate and the temperature, respectively

$$\varepsilon^f = \underbrace{(D_1+D_2\exp(D_3\sigma^*))}_{1}\underbrace{\left(1+D_4\ln\left(\frac{\dot{\varepsilon}}{\dot{\varepsilon}_0}\right)\right)}_{2}\underbrace{\left(1+D_5\left(\frac{T-T_a}{T_f-T_a}\right)\right)}_{3} \tag{2}$$

σ^* ($\sigma^* = \frac{\sigma_h}{\sigma_{vm}}$) represents the rate of triaxiality. σ_h and σ_{vm} represent respectively the hydrostatic stress and von Mises stress. Parameters D_1, D_2, D_3, D_4, D_5 are the five coefficients to be identified.

A separate study has been carried out with the objective of identifying these parameters. In order to determine the mechanical behavior of the Ti17 titanium alloy in extreme conditions, compression and shear tests were carried out. The parameters of the damage model were identified using tensile, shear and compression tests. The tests cover a wide range of strain rates ($0.1\ s^{-1}$–$10\ s^2$) and temperatures (25–800 °C). The results of this identification are summarized in Table 1.

2.1. Friction modeling

In order to model the contact at the tool/chip interface, a radial tribometer has been designed based on the work of [3,31,1,26]. Friction tests have been carried out under different conditions (dry, conventional lubrication and high-pressure lubrication) and over a wide range of speeds and lubrication pressures. Fig. 1 shows

the evolution of the apparent friction coefficient (macroscopic friction coefficient) as a function of the sliding speed. The apparent friction coefficient can be written as per Eq. (3), where F_t, F_n are the tangential force and the normal force. μ_{plas} represents the contribution due to plastic deformation

$$\mu_{app} = \frac{F_t}{F_n} = \mu_{adh} + \mu_{plas} \tag{3}$$

The identification of the adhesive friction coefficient ($\mu_{adh} = f(V)$) has been achieved using an inverse method. Based on numerical simulations, the adhesive friction coefficient can be approximated by the following relation: $\mu_{adh} \simeq 0.9\mu_{app}$.

2.2. Geometric model

First of all a multi-part conventional cutting model has been established based on the work done by [22] (Fig. 2). In order to optimize the computing time and to ensure the accuracy of the numerical simulations, a study concerning the sensitivity to the finite element mesh size has been performed. For this, the number of elements in Zones 1 and 2 have been varied. Reduced integration elements with eight nodes (C3D8RT) have been used in this study. The use of reduced integration is required in order to maintain reasonable calculation times. However, it is necessary to control the Hourglass. The study by [2] details the influence of different numerical parameters and the control of the deformation energy.
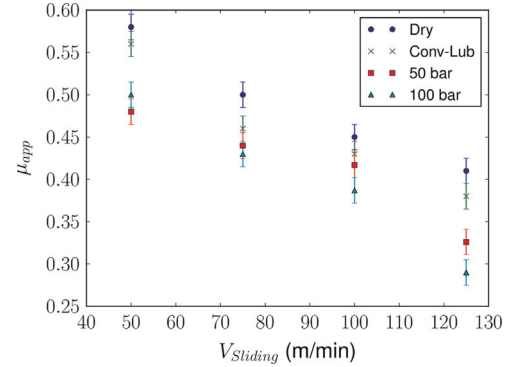

Fig. 1. Evolution of the apparent friction coefficient as a function of the friction velocity, for different lubrication conditions (Ti-17 Titanium alloy).
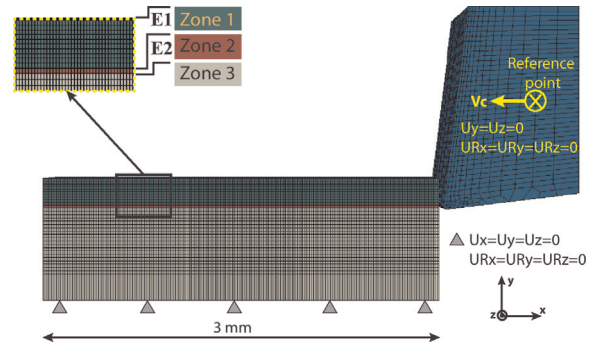

Fig. 2. Convnetional cutting model.

Table 1
Johnson–Cook behavior law and damage model parameters (Ti-17 Titanium alloy).

A (MPa)	B (MPa)	n	C	m	$\dot{\varepsilon}_0$ (s^{-1})	D_1	D_2	D_3	D_4	D_5
1012	399	0.22	0.035	0.85	10^{-1}	-0.2	0.34	-0.5	-0.035	2.7

Table 2
Model sensitivity to the mesh size ($f=0.2$ mm/rev, $V_C=75$ m/min).

Elements number	Mesh 1	Mesh 2	Mesh 3
Zone (E1,E2) (Z-axes)	10	7	5
Zone E1 (Y-axes)	10	10	10
Zone E2 (Y-axes)	2	2	1
Total (model)	100 996	78,047	42,448
Computational time	8 h:50	4 h:53	2 h:31
Average cutting force F_C (N)	1750	1790	1730

Table 3
Simulated conditions.

V_C (m/min)	75
feed rate (mm/rev)	0,1
Lubrication	conventional (12 m/s), 50 bar (80 m/s), 100 bar (113 m/s), 100 bar ($h=0$)

Thus, the total number of integration points has been varied between 42,448 and 100,996. Parallel computing on four processors using double precision option has been performed. Table 2 summarizes the main simulation conditions and results.

For the high-pressure water-jet assistance (HPWJA) model, a fluid part has been added (using an Eulerian mesh). In order to maintain reasonable computation times, the Eulerian field only covers the zone of the fluid/structure interaction. Fig. 3 presents the new model and Fig. 4 illustrates a simulation example Table 3.

2.3. Contact and boundary conditions

Contact management is handled simultaneously by two algorithms. A master–slave algorithm for the tool/chip contact and the general contact algorithm for the fluid/structure interaction.

Boundary conditions and initial conditions are presented in Fig. 3. The calculated fluid velocity V_{fluid} is applied as shown in Fig. 3. The nozzle diameter is 1 mm. The tool is fixed, only the workpiece moves in the X direction. The impact distance between the water-jet and the cutting edge is 0.5 mm. The geometrical parameters of the model have been fixed in order to focus on the mechanical and the thermal effects of the water-jet.

Simulations have been carried out using a high performance cluster. The total calculation time is between 30 h and 40 h (using two processors). It is necessary to point out that increasing the number of processors does not necessarily reduce the calculation time due to the use of the two contact algorithms.

It can be noted that in some conditions notably when the mesh is too coarse, there is penetration of the nodes from the Eulerian mesh into the Lagrangian structure. ABAQUS uses the penalty method to handle such problems. A mesh refinement is therefore strongly recommended. But, these recommendations are difficult to apply in machining. Fig. 5 illustrates some of the encountered problems (for a coarse and fine mesh).

2.4. Heat transfer

With version 6.10 of ABAQUS, heat transfer between a fluid and a structure is not supported. Without proper development by the
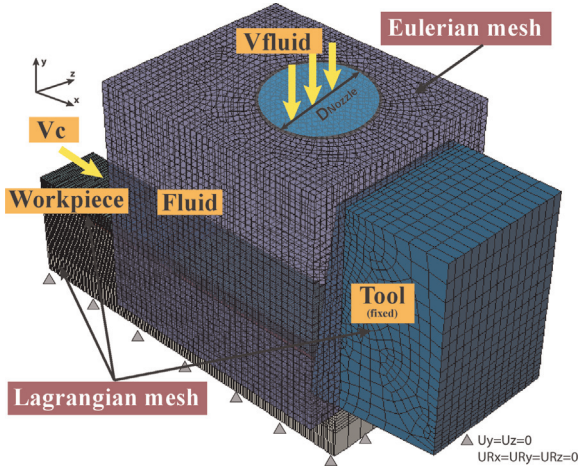

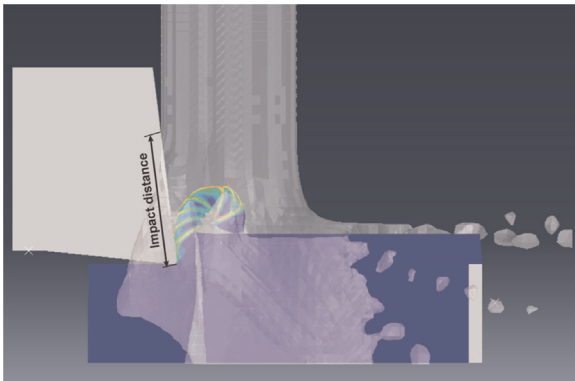**Fig. 3.** High-pressure water-jet model.

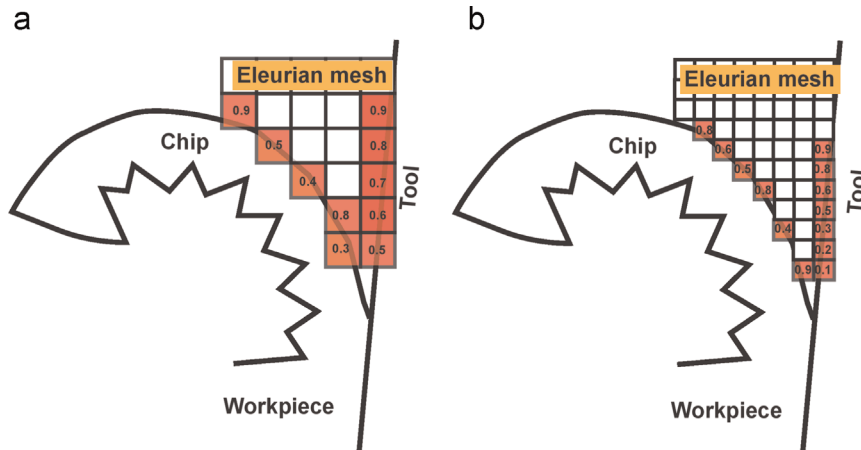**Fig. 4.** Example of the simulation of HPWJA.

Fig. 5. (a) Coarse mesh, (b) fine mesh.

user ABAQUS 6.10 does not simulate the effect of the water-jet on the temperature fields of the workpiece and the tool.

In order to ensure that heat transfer, an algorithm has been established. The idea consists of decomposing the total computation time t into Δt_i increments. The nodes on the structure in contact with the fluid are identified via the contact pressure. Nodes are considered to be in contact with the fluid if the contact pressure exceeds a threshold value. Once these nodes have been identified, a convection boundary condition is applied to them. The heat transfer coefficient is considered to depend on the fluid flow velocity. It is therefore necessary to first estimate, the fluid velocity at the nozzle outlet. It is calculated using Eq. (4), where P, ρ, η are the water-jet pressure, the density of the water and the efficiency of the nozzle, respectively

$$V = \eta \sqrt{\frac{2P}{\rho}} \tag{4}$$

Secondly, the Reynolds number is calculated using
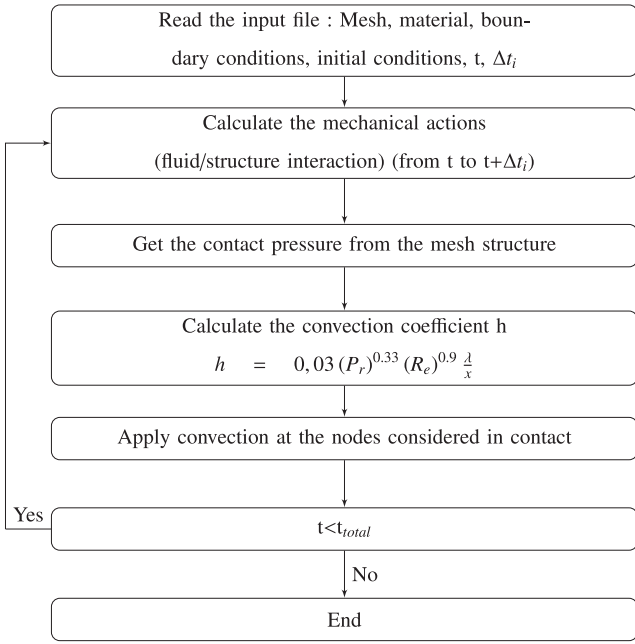
$$R_e = \frac{\rho V x}{\mu} \tag{5}$$

where μ, x, V are the dynamic viscosity, the distance traversed by the fluid and the fluid velocity, respectively. Then, using Eq. (6), the Prandtl number is calculated, where λ is the thermal conductivity and C_p is the heat capacity

$$P_r = \frac{C_p \mu}{\lambda} \tag{6}$$

Finally, the heat exchange coefficient h is calculated via Eq. (7) [27].

$$h = 0.03 \left(\frac{C_p \mu}{\lambda}\right)^{0.33} \left(\frac{\rho V x}{\mu}\right)^{0.9} \frac{\lambda}{x} \tag{7}$$

Fig. 6 describes the algorithm developed for this purpose.

Fig. 7 shows an example of the application of this algorithm. The convection boundary condition has been applied at the nodes where the contact pressure is greater than 0 MPa. Fig. 7(a) shows the contact pressure distribution and Fig. 7(b) shows the temperature distribution after the application of the convection boundary condition.

2.5. Comparison between numerical simulations and experimental tests

In order to investigate the influence of different cutting conditions and assistance parameters (i.e. nozzle diameter and pressure), orthogonal cutting tests have been carried out. Fig. 8 shows the experimental setup.

The comparison is mainly based on the cutting force. Table 2 highlights the fact that the results predicted by the model correspond to the experimental range: $F_{C_{exp}} = 1720 \pm 100$ N, $f = 0.2$ mm /rev ($F_{C_{exp}} = 1080 \pm 50$ N, $f = 0.1$ mm/rev). Moreover, the chip morphologies with/without high-pressure water-jet assistance are similar to those observed in the experimental tests. Fig. 9 shows the simulated fragmented chips. On the basis of this result, mesh 3 has been selected.

2.5.1. Results

Different simulations in different lubrication conditions have been conducted to investigate the effect of the water-jet on the thermal and mechanical fields in the tool and the workpiece. Table 1 summarizes the simulated conditions.

In order to decouple the thermal effect and the mechanical effect of the water-jet, simulations with and without heat transfer ($h=0$) have been carried out. Fig. 10 shows the temperature field on the rake face of the tool for the different lubrication conditions. An increase in the water-jet pressure increases the fluid velocity and thus the convection coefficient h. That is why a significant
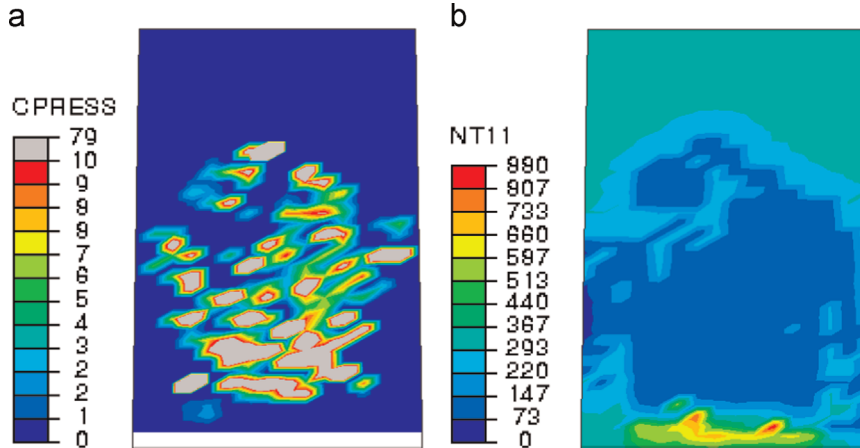

Fig. 6. Thermal coupling algorithm.

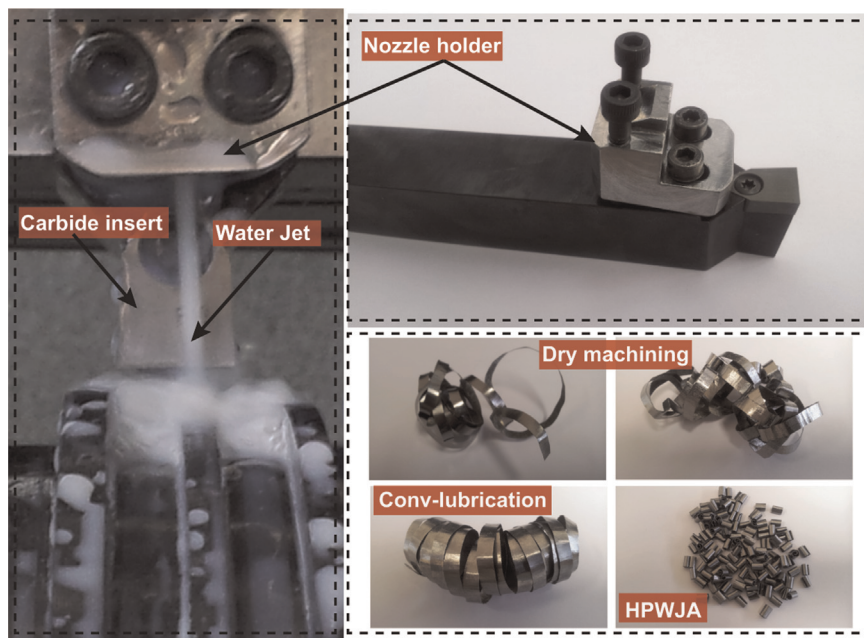**Fig. 7.** (a) Contact pressure field (tool rake face). (b) Temperature field.
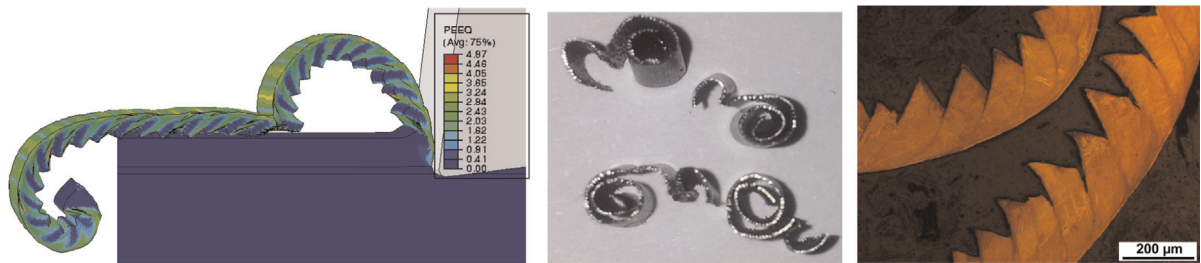
Fig. 8. Experimental setup.

Fig. 9. Chip fragmentation and morphology ($P = 100$ bar).

decrease in temperature can be seen for greater pressures. Indeed, this increase in pressure also allows the water-jet to have greater access to the tool/chip interface (i.e. reduced contact length at the tool/chip interface).

However, the tool tip temperature does not seem to be very influenced by water-jet assistance. Fig. 11 shows the temperature evolution of the tool tip for the pressure of 100 bar and for conventional lubrication. A slight decrease, which remains low, is observed.

The evolution of the temperature along the tool rake face (Fig. 10(d)) is shown in Fig. 12. The comparison between conventional lubrication and HP lubrification (100 bar) shows that the temperature drops about 400 °C at a distance of 0.1 mm from the cutting edge and about 200 °C at a distance of 0.2 mm. Hence, water-jet assistance ensures more efficient cooling. In fact, the high water-jet pressure does not cool the tool tip (Fig. 11) but increases dramatically the thermal gradient along the cutting face (Fig. 12).

With conventional lubrication, the chip form is continuous and in the shape of "ribbons". Increasing the pressure causes the application of greater force on the chip which deforms and breaks when the stress reaches the rupture value. It is important to note that the chips are broken at the primary shear bands as these are the most strongly deformed zones, which have undergone the greatest damage. Fig. 13 illustrates these observations.

Fig. 13 (c) and (d) illustrates the effect of decoupling the thermal effect and the mechanical effect of the water-jet. In fact, the fragmented chip shown in Fig. 13(c) has been obtained via the combination of mechanical effects (fluid/structure interaction) and the thermal effect (heat transfer). However, the result in which the thermal effect has been removed ($h = 0$) is illustrated by Fig. 13 (d) which shows a highly deformed chip. In this case the chip has not been fragmented. Without heat transfer between the chip and the water-jet, the chip temperature is around 400–500 °C. At these temperature levels, thermal softening of the material takes place. So, greater deformation is possible before the rupture. Fig. 14 illustrates the chip morphology for several computing times ($P = 100$ bar).

The contact at the tool/chip interface (Z_{II}) is shown in Fig. 15. The results of the different simulations show that with water-jet assisted machining (100 bar) the average temperature of the interface, except the area in contact with the tip of the tool, decreases by about 300 °C compared to conventional machining. Fig. 15(c) shows that without the including the thermal effect ($h = 0$) the temperature also decreases. The cooling is therefore due not only to the thermal effect but also to the mechanical effect of the water-jet. Indeed, by reducing the contact length at the tool/chip interface via the mechanical action of the water-jet, the friction zone (Z_{II}) decreases thereby limiting frictional heating. Indeed, the contact length decreases from about 0.19 mm in
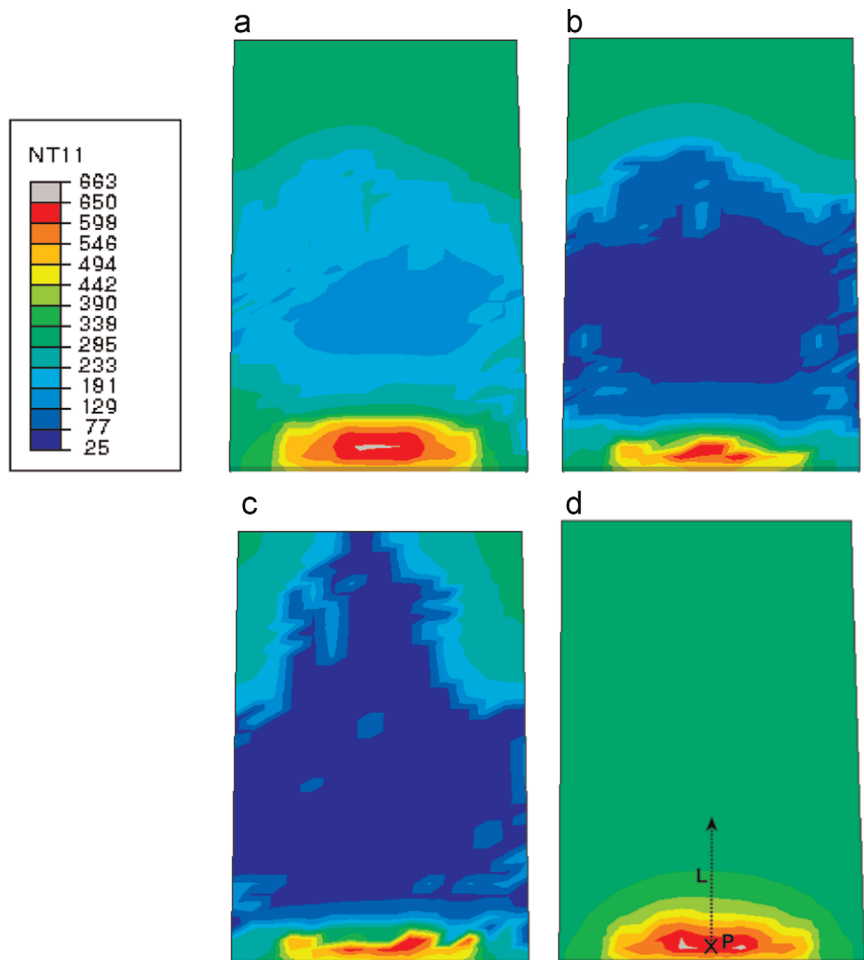
Fig. 10. Temperature field in the tool (a) conventional lubrication, (b) $P=50$ bar, (c) $P=100$ bar, (d) $P=100$ bar ($h=0$).
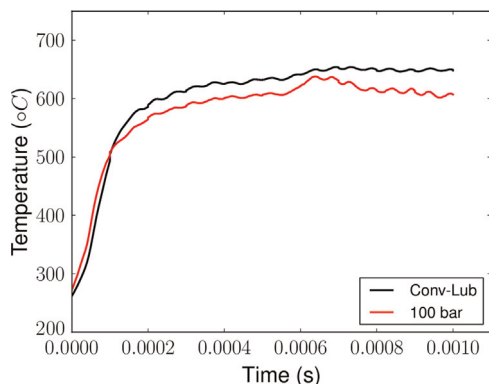

Fig. 11. Evolution of the temperature in the cutting edge.
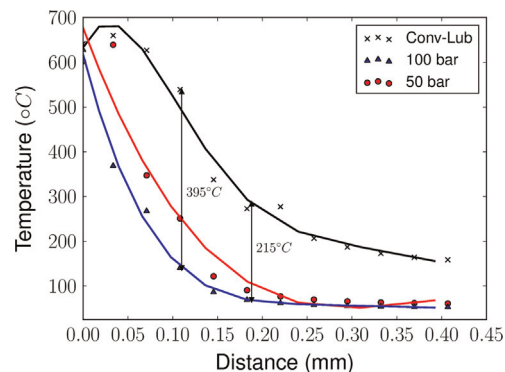

Fig. 12. Evolution of the temperature along the tool rake face.

conventional machining to about 0.13 mm with high-pressure water-jet assistance.

3. Conclusion

In this study a HPWJA model has been developed. The model is based on the CEL technique. To ensure the heat transfer between the fluid and the structure a specific algorithm has been developed. The comparison between the experimental results and the numerical simulations show that the model provides good predictions for the cutting forces, the chip morphology and chip

fragmentation. Moreover, the friction model makes it possible to take into account the influence of the lubrication and the cutting speed.

Simulations have shown that water-jet assistance allows more efficient cooling of the cutting area when compared to conventional lubrication, but the decrease in temperature at the tool tip is not significant. However, the decrease in temperature can reach upto 400 °C at a distance of about 0.1 mm from the tool tip. In addition, under the action of the water-jet, the tool/chip contact length is reduced by approximately 30%. Hence, limiting the frictional heating.
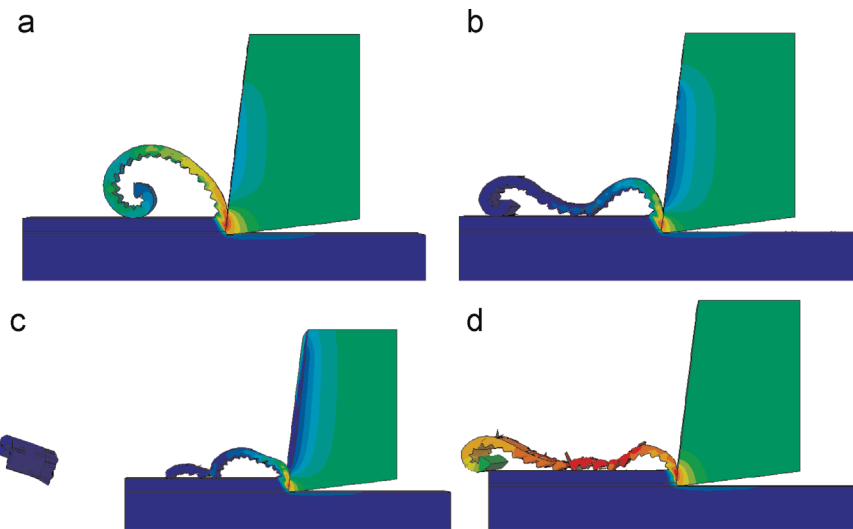
Fig. 13. Temperature field: (a) Conventional lubrication, (b) $P=50$ bar, (c) $P=100$ bar, (d) $P=100$ bar ($h=0$).
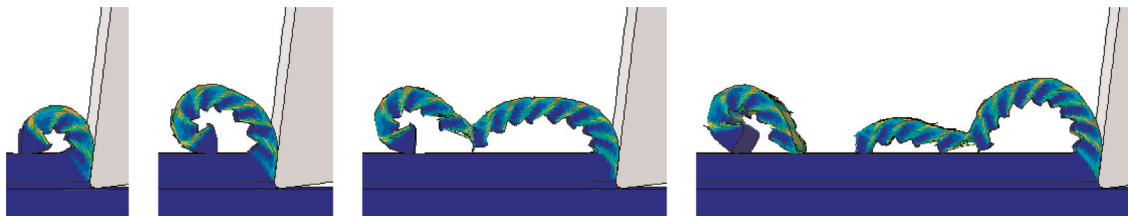

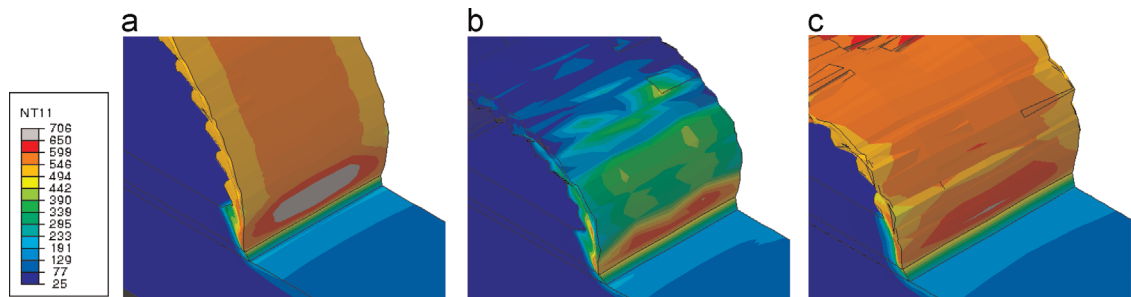**Fig. 14.** Chip morphology for several computing times.

Fig. 15. Temperature field: (a) conventional machining (without lubrication), (b) $P=100$, (c) $P=100$ bar ($h=0$).

The possibility of decoupling the thermal and mechanical effects due to the water jet gives a very interesting way of assessing the real factors influencing the cutting process. In particular, the influence of the two effects on chip fragmentation was investigated. It was concluded that fragmentation is ensured by the combination of the two effects.

Acknowledgments

References

[1] H.B. Abdelali, C. Claudin, J. Rech, W.B. Salem, P. Kapsa, A. Dogui, Experimental characterization of friction coefficient at the tool-chip-workpiece interface during dry cutting of aisi 1045, Wear 286–287 (2012) 108–115, tribology in Manufacturing Processes.

[2] M. Barge, Etude expérimentale et numérique des mécanismes de coupe par abrasion (Ph.D. thesis), Ecole Centrale de Lyon, 2005.

[3] C. Bonnet, F. Valiorgue, J. Rech, C. Claudin, H. Hamdi, J. Bergheau, P. Gilles, Identification of a friction model-application to the context of dry cutting of an aisi 316l austenitic stainless steel with a tin coated carbide tool, Int. J. Mach. Tools Manuf. 48 (11) (2008) 1211–1223.

[4] S. Buchkremer, B. Wu, D. Lung, S. Münstermann, F. Klocke, W. Bleck, Fe-simulation of machining processes with a new material model, J. Mater. Process. Technol. 214 (3) (2014) 599–611.

[5] C.-W. Chang, C.-P. Kuo, Evaluation of surface roughness in laser-assisted machining of aluminum oxide ceramics with Taguchi method, Int. J. Mach. Tools Manuf. 47 (1) (2007) 141–147.

[6] M. Chizari, S. Al-Hassani, L. Barrett, Experimental and numerical study of water jet spot welding, J. Mater. Process. Technol. 198 (1–3) (2008) 213–219.

[7] M. Chizari, L. Barrett, S. Al-Hassani, An explicit numerical modeling of the water jet tube forming, Comput. Mater. Sci. 45 (2) (2009) 378–384.

[8] C. Courbon, V. Sajn, D. Kramar, J. Rech, F. Kosel, J. Kopac, Investigation of machining performance in high pressure jet assisted turning of inconel 718: a numerical model, J. Mater. Process. Technol. 211 (11) (2011) 1834–1851.

[9] H. Ding, N. Shen, Y.C. Shin, Thermal and mechanical modeling analysis of laser-assisted micro-milling of difficult-to-machine alloys, J. Mater. Process. Technol. 212 (3) (2012) 601–613.

[10] H. Ding, Y.C. Shin, Laser-assisted machining of hardened steel parts with surface integrity analysis, Int. J. Mach. Tools Manuf. 50 (1) (2010) 106–114.

[11] G. Germain, P.D. Santo, J. Lebrun, Comprehension of chip formation in laser assisted machining, Int. J. Mach. Tools Manuf. 51 (3) (2011) 230–238.

[12] C.-Y. Hsu, C.-C. Liang, T.-L. Teng, A.-T. Nguyen, A numerical study on high-speed water jet impact, Ocean Eng. 72 (2013) 98–106.

[13] G. Johnson, W. Cook, A constitutive model and data for metals subjected to large strains, high strain rates and temperature, in: The Seventh International Symposium on Ballistics, 1983.

[14] G. Johnson, W. Cook, Fracture characteristics of three metals subjected to various strains, strain rates, temperatures and pressures, Eng. Fract. Mech. 21 (1) (1985) 31–48.

[15] M. Junkar, B. Jurisevic, M. Fajdiga, M. Grah, Finite element analysis of single-particle impact in abrasive water jet machining, Int. J. Impact Eng. 32 (7) (2006) 1095–1112.

[16] T. Kagnaya, L. Lambert, M. Lazard, C. Boher, T. Cutard, Investigation and fea-based simulation of tool wear geometry and metal oxide effect on cutting process variables, Simul. Model. Pract. Theory 42 (2014) 84–97.

[17] N. Kumar, M. Shukla, Finite element analysis of multi-particle impact on erosion in abrasive water jet machining of titanium alloy, J. Comput. Appl. Math. 236 (18) (2012) 4600–4610.

[18] B. Lesourd, Etude et modélisation des mécanismes de bandes de cisaillement en coupe des métaux. application au tournage assisté laser de l'alliage de titane ta6v (Ph.D. thesis), Ecole Centrale de NANTES, 1996.

[19] R. Liu, M. Salahshoor, S. Melkote, T. Marusich, The prediction of machined surface hardness using a new physics-based material model, in: 2nd CIRP Conference on Surface Integrity (CSI), Procedia CIRP, 2014, vol. 13, pp. 249–256.

[20] R. Liu, M. Salahshoor, S. Melkote, T. Marusich, A unified material model including dislocation drag and its application to simulation of orthogonal cutting of OFHC copper, J. Mater. Process. Technol. 216 (2015) 328–338.

[21] P. Ludwik, Elemente der technologischen mechanik, Springer, Berlin, Heidelberg, 1909 10.1007/978-3-662-40293-1.

[22] T. Mabrouki, F. Girardin, M. Asad, J.-F. Rigal, Numerical and experimental study of dry cutting for an aeronautic aluminium alloy (a2024-t351), Int. J. Mach. Tools Manuf. 48 (11) (2008) 1187–1197.

[23] T. Mabrouki, K. Raissi, Stripping process modeling: interaction between a moving waterjet and coated target, Int. J. Mach. Tools Manuf. 42 (11) (2002) 1247–1258.

[24] T. Mabrouki, K. Raissi, A. Cornier, Numerical simulation and experimental study of the interaction between a pure high-velocity waterjet and targets: contribution to investigate the decoating process, Wear 239 (2) (2000) 260–273.

[25] S.N. Melkote, R. Liu, P. Fernandez-Zelaia, T. Marusich, A physically based constitutive model for simulation of segmented chip formation in orthogonal cutting of commercially pure titanium, CIRP Ann.–Manuf. Technol. (2015), http://dx.doi.org/10.1016/j.cirp.2015.04.060.

[26] J. Rech, P. Arrazola, C. Claudin, C. Courbon, F. Pusavec, J. Kopac, Characterisation of friction and heat partition coefficients at the tool-work material interface in cutting, CIRP Ann. – Manuf. Technol. 62 (1) (2013) 79–82.

[27] W. Rohsenow, J. Hartnett, Y. Cho, Handbook of Heat Transfer, McGraw-Hill Professional, United States, 1998.

[28] F. Salvatore, S. Saad, H. Hamdi, Modeling and simulation of tool wear during the cutting process, in: The 14th CIRP Conference on Modeling of Machining Operations (CIRP CMMO), Procedia CIRP, vol. 8, 2013, pp. 305–310.

[29] S. Skvarenina, Y. Shin, Laser-assisted machining of compacted graphite iron, Int. J. Mach. Tools Manuf. 46 (1) (2006) 7–17.

[30] R.K. Yadav, K. Abhishek, S.S. Mahapatra, A simulation approach for estimating flank wear and material removal rate in turning of inconel 718, Simul. Model. Pract. Theory 52 (2015) 1–14.

[31] F. Zemzemi, J. Rech, W.B. Salem, A. Dogui, P. Kapsa, Identification of a friction model at tool/chip/workpiece interfaces in dry machining of AISI4142 treated steels, J. Mater. Process. Technol. 209 (8) (2009) 3978–3990.

[32] X. Zhang, R. Shivpuri, A. Srivastava, Role of phase transformation in chip segmentation during high speed machining of dual phase titanium alloys, J. Mater. Process. Technol. 214 (12) (2014) 3048–3066.

[33] Y. Ayed, G. Germain, W. Ben Salem, H. Hamdi, Experimental and numerical study of laser-assisted machining of Ti6Al4V titanium alloy, Finite Elem. Anal. Des. 92 (2014) 72–79.